ELSEVIER

www.elsevier.com/locate/ophopt

Ophthal. Physiol. Opt. Vol. 21, No. 4, pp. 296–311, 2001

0275-5408/01/$20.00

PII: S0275-5408(00)00057-0

Optical and biometric relationships of the isolated pig crystalline lens

Abhiram S. Vilupuru and Adrian Glasser

College of Optometry, 4901 Calhoun Road, University of Houston, Houston, TX 77004, USA

Summary

Aim: To investigate the interrelationships between optical and biometric properties of the porcine crystalline lens, to compare these findings with similar relationships found for the human lens and to attempt to fit this data to a geometric model of the optical and biometric properties of the pig lens.

Methods: Weight, focal length, spherical aberration, surface curvatures, thickness and diameters of 20 isolated pig lenses were measured and equivalent refractive index was calculated. These parameters were compared and used to geometrically model the pig lens.

Results: Linear relationships were identified between many of the lens biometric and optical properties. The existence of these relationships allowed a simple geometrical model of the pig lens to be calculated which offers predictions of the optical properties.

Conclusions: The linear relationships found and the agreement observed between measured and modeled results suggest that the pig lens confirms to a predictable, preset developmental pattern and that the optical and biometric properties are predictably interrelated. © 2001 The College of Optometrists. Published by Elsevier Science Ltd. All rights reserved.

Introduction

Pig lenses have previously been used for measurements of spherical aberration (Sivak and Kreuzer, 1983) and chromatic aberration (Kreuzer and Sivak, 1985). Despite these studies, there are to our knowledge no other studies which quantify and compare the optical and biometric properties of pig lenses. A detailed study of the pig lens has been undertaken to compare the results from this mammalian crystalline lens with the results obtained from similar studies of the human lens (Glasser and Campbell, 1998, 1999). The pig lens is used frequently in ophthalmology training of surgical techniques as well as being used for research on intraocular lens design (Hara *et al.*, 1990), and towards understanding the requirements for polymer refilling of the capsular bag (Hettlich *et al.*, 1994), but little is known about its optical properties.

In any species, the crystalline lens is an unusual organ in that, it grows through out life, continuously adding new fiber shells (Kuszak and Brown, 1994). Pierscionek and Augusteyn (1991) suggest that under such dynamic conditions various optical and physical properties of the lens must constantly change. In this regard, it is of interest to know if the relationship between optical and biometric lens parameters follows a preset developmental pattern. Interrelationships between the optical properties (focal length, spherical aberration) and the biometric parameters (weight, lens surface curvatures, thickness and diameter) may be expected. Indeed, in the human lens various optical, biometric and physical properties, and their age changes show some striking relationships (Glasser and Campbell, 1998, 1999). One of the strongest linear relationships identified from the human lens experiments, lens focal length and equatorial diameter, suggests that growth and development of the human lens may be optically and biometrically constrained. Similar information has until now been unavailable for the porcine lens.

Further, although the mammalian lens gradient refractive

Received: 6 September 1999
Revised form: 29 November 2000
Accepted: 4 December 2000

Correspondence and reprint requests to: Adrian Glasser. Tel.: +1-713-743-1876; fax: +1-713-743-2053.
E-mail address: aglasser@popmail.opt.uh.edu (A. Glasser).

index has been studied from elliptical crystalline lens models (Nakao *et al.*, 1968; Nakao *et al.*, 1969; Masajada, 1999), these are theoretical and not empirically based models. Quantifying and understanding the various optical and biometric relationships of the readily available and frequently used, but infrequently studied, pig crystalline lens will facilitate future studies and understanding of the gradient refractive index of the mammalian lens.

This study has been undertaken to: (a) explore the optical and biometric relationships of the pig lens, (b) compare and contrast the interrelationships between these parameters with similar data from human lenses and (c) generate a geometrical model of the porcine lens from the measured parameters to test the predictive ability of the model.

Methods

Twenty porcine eyes were obtained from a slaughter house by a supplier (Vision Tech, Dallas, TX). Eyes were enucleated, placed in saline and shipped overnight on ice. The age of the pigs at the time of slaughter was unknown. Upon arrival within 24 h of sacrifice, the eyes were placed in a dissecting dish filled with buffered saline of the following composition (g/l) NaCl 8.00, KCl 0.40, Na_2HPO_4 0.10, sucrose 1.00, Hepes 2.38 buffered with 10 m NaOH to a pH of 7.4. The cornea was removed, the anterior sclera was cut through and the lens along with a portion of ciliary body tissue was removed from the globe. The vitreous adhering to the posterior lens surface was removed. The zonule was cut and the ciliary body was separated from the lens taking care to not rupture the lens capsule.

The isolated lens wet weight was measured three times in succession and the average weight was recorded. The focal length and spherical aberration of the isolated lenses were measured using a scanning laser apparatus similar to that described previously (Glasser and Campbell, 1999). To do this, the lens was placed on a molding clay pedestal on its equatorial edge with the anterior surface facing forward in a glass chamber ($8 \times 4 \times 4$ cm) filled with buffered saline (Glasser and Campbell, 1998). A 6 mW He-Ne laser (633 nm) beam was reflected off mirrors mounted on x–y stepper-motor stages and directed through the front window of the glass chamber to enter the anterior surface of the lens parallel with the lens optical axis. The laser was scanned horizontally across the full diameter of the lens so that a total of 51 laser beams were incident on and refracted by the lens. At each step in the laser scan, an image of the laser beam passing through the lens was captured via a video camera connected to a computer and mounted above the lens. The laser beam path was digitized to record the slopes and intercepts for each entrance and exit beam (Glasser and Campbell, 1998, 1999).

Custom software was used to analyze the data obtained from the scanning laser apparatus. The points of intersection of the entrance and exit beams are the principal points (*Figure 1a*). The optical axis is defined by the beam that passes through the lens undeviated. Mean total focal length (as opposed to paraxial focal length) was calculated as the average distance traversed by all refracted exit beams from their principal points to their points of intersection with the optical axis (*Figure 1a*). All focal length measurements were with reference to the 633nm wavelength laser beam. An estimate of the dioptric power of the lens (F) was obtained from the lens focal length (f) and the refractive index of the saline ($n = 1.3333$) from the following equation:

$$F = \frac{(n \times 1000)}{f} \tag{1}$$

The extent of the spherical aberration of the lenses was determined by fitting second or higher order polynomials to all the intersection points of the exit beams with the optical axis as a function of the normalized lens equatorial diameter (*Figure 1b*) (Glasser and Campbell, 1998, 1999). These polynomials describe the change in the focal distance of each exit beam as a function of the full diameter of the lens. The difference between the average focal power at the two equatorial edges of the lens ($x = -1$ and $x = 1$) and the focal power at the center of the lens ($x = 0$) gives the extent of the spherical aberration of the lens in diopters. The paraxial focal length of the lens was obtained from the solution of this spherical aberration polynomial at zero (i.e. at the optical axis).

Immediately following the laser scan measurements, lens profile images were captured (*Figure 1c*). While the lens remained immobile in the chamber in the molding clay, an image of the lens profile was capture with the CCD video camera mounted above the lens and saved to disk. Camera magnification was determined by capturing an image and measuring graph paper at the plane of focus of the camera. After the lens profile image was captured and the calibration applied, approximately 40 points were manually marked along the entire extent of the anterior and posterior surfaces to the lens equator via the mouse cursor using image analysis software (Optimas, Media Cybernetics, WA) (*Figure 1d*). The coordinates of these points were saved to disk and the anterior and posterior lens surface radii of curvature were obtained by fitting spherical curves to this data. The lens sagittal thickness and equatorial diameter were also measured from the digitized lens images.

Retrospectively, the accuracy of measuring the lens surface curvatures, lens thickness and lens diameters from digitized images was tested by measuring steel ball bearings of known dimensions in the same way. Four ball bearings with radii of curvature similar in magnitude to the pig lens radii of curvatures were used. The ball bearing anterior and posterior surface curvatures, thickness and diameters were measured from digitized

a

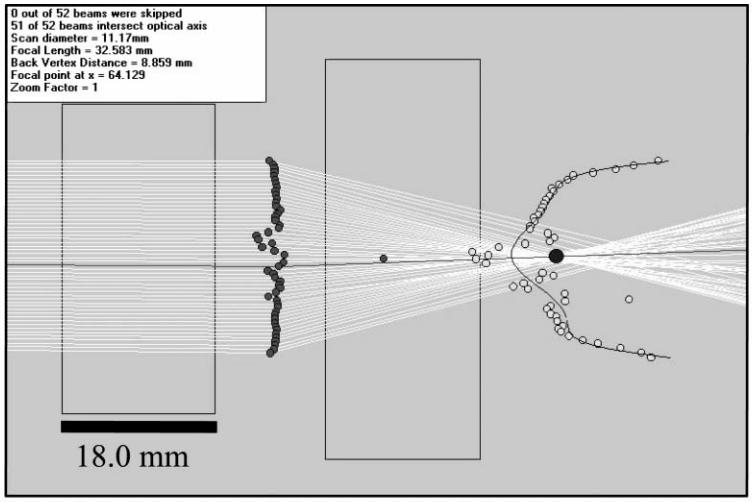
0 out of 52 beams were skipped
51 of 52 beams intersect optical axis
Scan diameter = 11.17mm
Focal Length = 32.583 mm
Back Vertex Distance = 8.859 mm
Focal point at x = 64.129
Zoom Factor = 1
18.0 mm

b

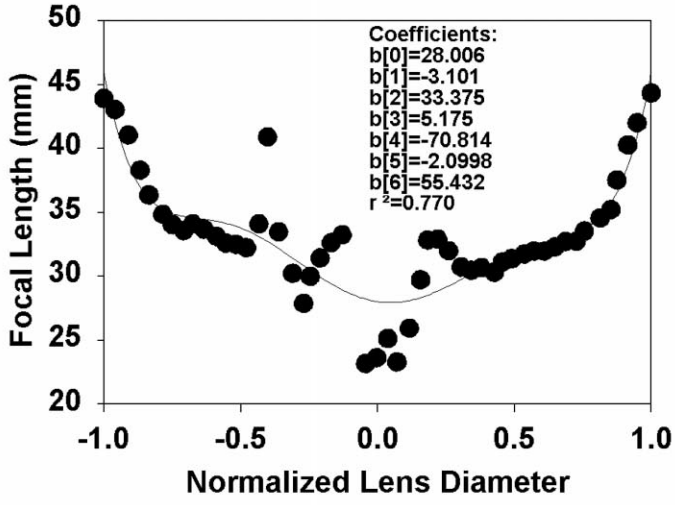
Coefficients:
b[0]=28.006
b[1]=-3.101
b[2]=33.375
b[3]=5.175
b[4]=-70.814
b[5]=-2.0998
b[6]=55.432
r ²=0.770
Focal Length (mm)
50
45
40
35
30
25
20
-1.0
-0.5
0.0
0.5
1.0
Normalized Lens Diameter

c

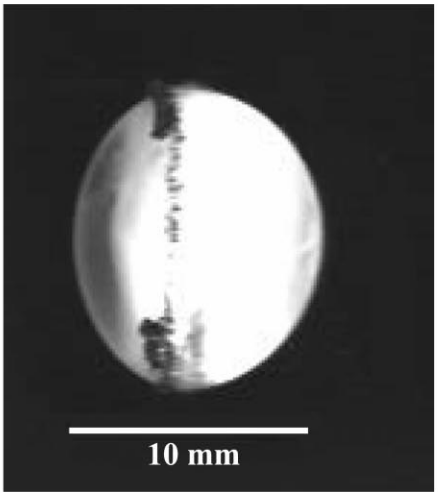
10 mm

d

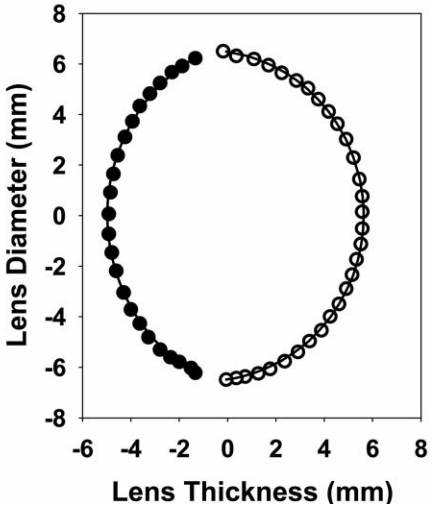
Lens Diameter (mm)
8
6
4
2
0
-2
-4
-6
-8
-6
-4
-2
0
2
4
6
8
Lens Thickness (mm)

images as described for the pig lenses. Graphs of the ball bearing actual versus measured surface curvatures, diameters and thickness were plotted (not shown). In addition, the volumes of the ball bearings were calculated and compared with the ball bearing volumes calculated directly from the known ball bearing radii of curvatures, thickness and diameters.

The equivalent refractive index of each pig lens was calculated using an iterative solution to the following equations as described previously (Glasser and Campbell, 1999):

$$F = (F_1 + F_2) - \frac{(t \times F_1 \times F_2)}{n_2} \tag{2}$$

where

$$F_1 = \frac{(n_2 - n_1)}{r_1} \tag{3}$$

and

$$F_2 = \frac{(n_3 - n_2)}{r_2} \tag{4}$$

Where F is the focal power measured using the scanning laser, F_1 is the anterior surface power and F_2 is the posterior surface power, r_1 = anterior radius of curvature, r_2 = posterior radius of curvature, $n_1 = n_3$ = refractive index of the saline (1.3333), t = sagittal thickness of the lens and n_2 = the unknown equivalent refractive index of the lens. Both the total and paraxial equivalent refractive index values were calculated using the total and paraxial focal lengths respectively. In addition, the total lens powers were calculated for each lens from the surface curvatures (r_1 and r_2) and the lens thickness measurement (t) assuming an equivalent refractive index of 1.4955 (the mean value obtained from all pig lenses in this study, as described above; see the Results section) and again assuming a value of 1.5088 (Kreuzer and Sivak, 1985; Coile and O'Keefe, 1988) using Eq. (2).

Since the full extents of the anterior and posterior surfaces of the porcine lens were well fitted with spherical curves, lens volume was calculated by adding the volume of the anterior cap and the volume of the posterior cap using the following formula:

$$\text{Volume} = \left[\frac{\pi}{3} \times (h_{\text{ant}})^2 \times (3t_{\text{ant}} - h_{\text{ant}})\right] + \left[\frac{\pi}{3} \times (h_{\text{post}})^2 \times (3r_{\text{post}} - h_{\text{post}})\right] \tag{5}$$

where h_{ant} = height of the anterior cap, r_{ant} = radius of curvature of the anterior surface; h_{post} = height of the posterior cap; r_{post} = radius of curvature of the posterior surface. The heights of the anterior and posterior caps were calculated geometrically from the intersection points of the two circles describing the anterior and posterior radii of curvature and the thickness of the lens. The density of the lens was also calculated using the formula:

$$\text{Density} = \frac{\text{weight}}{\text{volume}} \tag{6}$$

Lens modeling

Since the lens surface curvatures were well represented by spherical curves and many significant linear relationships were found between the various optical and biometric variables measured (see the Results section), a geometric model of the porcine lens was created using a VisualBasic program (*Figure 2*). The geometric model was based on anterior radius, posterior radius and thickness. The lens diameter was calculated geometrically from these three values and using a given equivalent refractive index value, the modeled lens focal length was calculated from Eqs. (2), (3) & (4).

Anova and orthogonal regressions (*JMP Statistics and Graphics Guide*, *Version 4*, 2000) were calculated to determine p-values and show that they were for the most part less than 0.05. Orthogonal regressions (rather than linear regressions) were used to compare various optical and biometric parameters since neither variable could be considered as a dependent variable. Unless otherwise mentioned all the regressions used are orthogonal regressions. An α value of 0.05 was considered significant.

Figure 1. (a) A laser is scanned horizontally across the full diameter of the lens in 51 discreet steps. The beam passing undeviated through the lens is the optical axis (dark horizontal line). The points of intersection of all entrance and exit beams are the principal points of the lens (filled symbols). The black boxes to the left and right of the principle plane identify the regions in which the entrance and exit beams are located during the scan. The larger black symbol on the optical axis represents the average focal length of the lens. The points of intersection of the exit beams with optical axis (open symbols) represent the spherical aberration of the lens. (b) The extent of the spherical aberration was obtained by fitting an even order polynomial (here 6th order) to all the points of intersection of the exit beams with the optical axis as a function of the normalized equatorial diameter of the lens. (c) Profile image of the isolated pig lens in saline as viewed by a video camera from above. (d) Anterior and posterior lens surface curvatures. Points were marked along the surfaces of the lens image with a mouse cursor (filled symbols: anterior surface; open symbols: posterior surface). These points were fitted with spherical fits (solid lines) to obtain the lens anterior and posterior radii of curvature. The lens shown here is 10.49 mm thick.

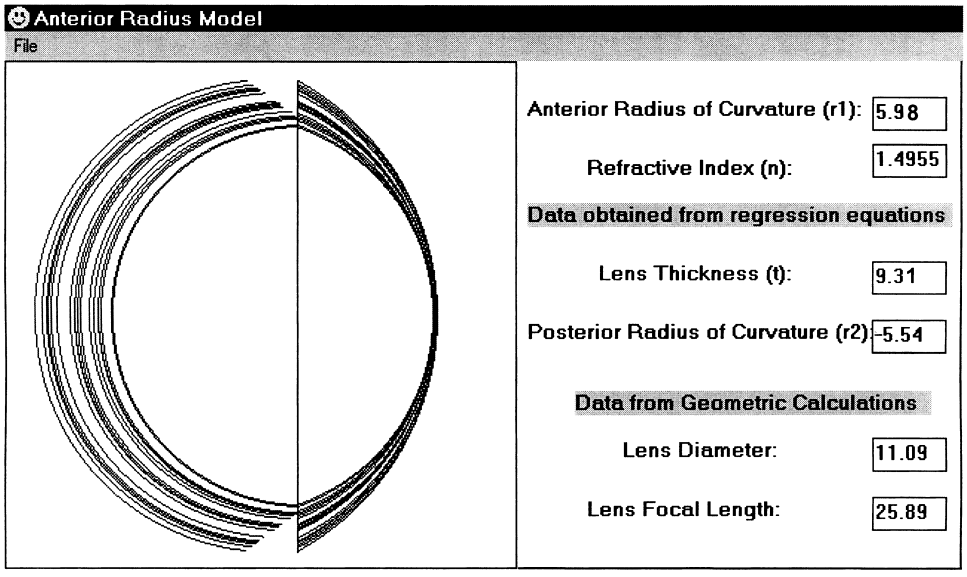

Figure 2. Output window from a VisualBasic program showing the anterior radius model of all pig lenses used. The measured lens anterior radius of curvature and the equivalent refractive index (1.4955) of the lens are input parameters. Posterior radius and thickness are then calculated from the linear regression equations and the calculated lens diameter and focal length are the output parameters. The graphic window shows the modeled lenses for all 20 pig lenses used in this study. A similar procedure was used (not shown) to calculate the lenses using thickness and equivalent refractive index as the input parameters (lens thickness model).

Results

Retrospective analysis of digitized images of four ball bearings of known dimensions showed that the measured anterior, posterior radii of curvature, thickness and diameters differed systematically from the actual values. Plots of the measured versus actual ball bearing dimensions showed that, although significantly linearly correlated, these relationships did not fall systematically along the one-to-one lines. From the slopes and regressions from these plots, correction factors could be calculated for the anterior, posterior radii of curvature, thickness and diameter measurements. After applying these corrections to the ball bearing radii of curvatures and thickness, the ball bearing volumes were calculated (Eq. (5)) and compared to the known volumes. Based on these findings, the same corrections were applied to the measured pig lens anterior, posterior radii, thickness and diameters. All the pig lens data presented are for the values corrected in this way.

Lenses were obtained from pigs of unknown ages, from populations of younger (~3–5 years) and older (~5–8 years) pigs. Since the mammalian crystalline lens grows continuously throughout life, the wet weights (min = 0.55 g; mean = 0.78 g; max = 1.08 g) suggest that the lenses were from pigs of a range of different ages.

The entire diameter of the lens anterior and posterior surface curvatures were well fitted with spherical curves. The range of r^2 values for the spherical fits of anterior surface were 0.980–0.997, and for the posterior surface were 0.900–0.999.

Interrelationships between biometric properties of the lenses

The biometric properties measured were, weight, thickness, equatorial diameter, anterior and posterior radii of curvature. Significant orthogonal regressions between all of these measurements are shown in *Table 1* or *Figure 3*. As a function of increasing weight of the pig lens, there is a significant linear increase in anterior radius of curvature (*Figure 3a*), thickness, lens diameter, total focal length (*Figure 4a*) and a decrease in posterior radius of curvature. Since lens weight and diameter and lens weight and thickness are correlated, it follows that there is also a significant linear increase in lens diameter with thickness.

The isolated lens anterior and posterior radii of curvature are significantly linearly related (*Figure 3b*). With an increase in anterior radius of curvature there is an increase in posterior radius of curvature given by:

$$\text{Posterior radius of curvature} = -0.806 \times (\text{anterior radius of curvature}) - 0.667 \quad (7)$$

With increasing thickness, the porcine lenses show a linear increase in anterior radius of curvature (*Figure 3c*) and from Eq. (7), therefore also an increase (of negative sign) in posterior radius of curvature. In addition, as the

Table 1. Slope, intercept and r values for the orthogonal regression analysis between the various parameters measured for 20 pig lenses studied. Data not included in this table are included in the figures. Unless otherwise specified p-values are less than 0.05

$X\downarrow$ $Y\rightarrow$	Anterior radius of curvature	Posterior radius of curvature	Thickness	Equatorial diameter	Volume	Measured total focal length
Weight	–	slope = −2.175 intercept = −4.099 r = −0.850	slope = 4.121 intercept = 6.545 r = 0.849	slope = 4.951 intercept = 7.484 r = 0.824	slope = 788.484 intercept = 48.181 r = 0.864	–
Posterior radius of curvature	slope = −1.240 intercept = −0.826 r = −0.922	–	slope = −1.757 intercept = −0.432 r = −0.937	slope = −2.093 intercept = −0.834 r = −0.969	slope = −362.38 intercept = −1436.15 r = −0.971	–
Thickness	slope = 0.764 intercept = −1.093 r = 0.960	slope = −0.569 intercept = −0.246 r = −0.937	–	slope = 1.301 intercept = −1.355 r = 0.970	slope = 213.25 intercept = −1415.77 r = 0.989	–
Equatorial diameter	slope = 0.579 intercept = −0.213 r = 0.967	slope = −0.478 intercept = −0.398 r = −0.969	slope = 0.768 intercept = 1.042 r = 0.970	–	slope = 167.13 intercept = −1227.91 r = 0.978	slope = 2.587 intercept = −1.978 r = 0.927
Volume	slope = 0.004 intercept = 3.991 r = 0.961	slope = −0.0027 intercept = −4.0 r = −0.971	slope = 0.005 intercept = 6.694 r = 0.989	slope = 0.006 intercept = 7.353 r = 0.978	–	slope = 0.015 intercept = 17.668 r = 0.913
Paraxial focal length	slope = 0.147 intercept = 2.792 r = 0.503	slope = −0.2 intercept = −0.908 r = −0.537	slope = 0.411 intercept = −0.311 r = 0.452	slope = 0.280 intercept = 4.448 r = 0.582	slope = 80.07 intercept = −1296.51 r = 0.492	slope = 0.692 intercept = 10.480 r = 0.622
Paraxial focal length and paraxial refractive index: slope = −0.006 ntercept = 1.669 r = −0.856				Paraxial focal length and weight: slope = 0.046 intercept = −0.346 r = 0.557		

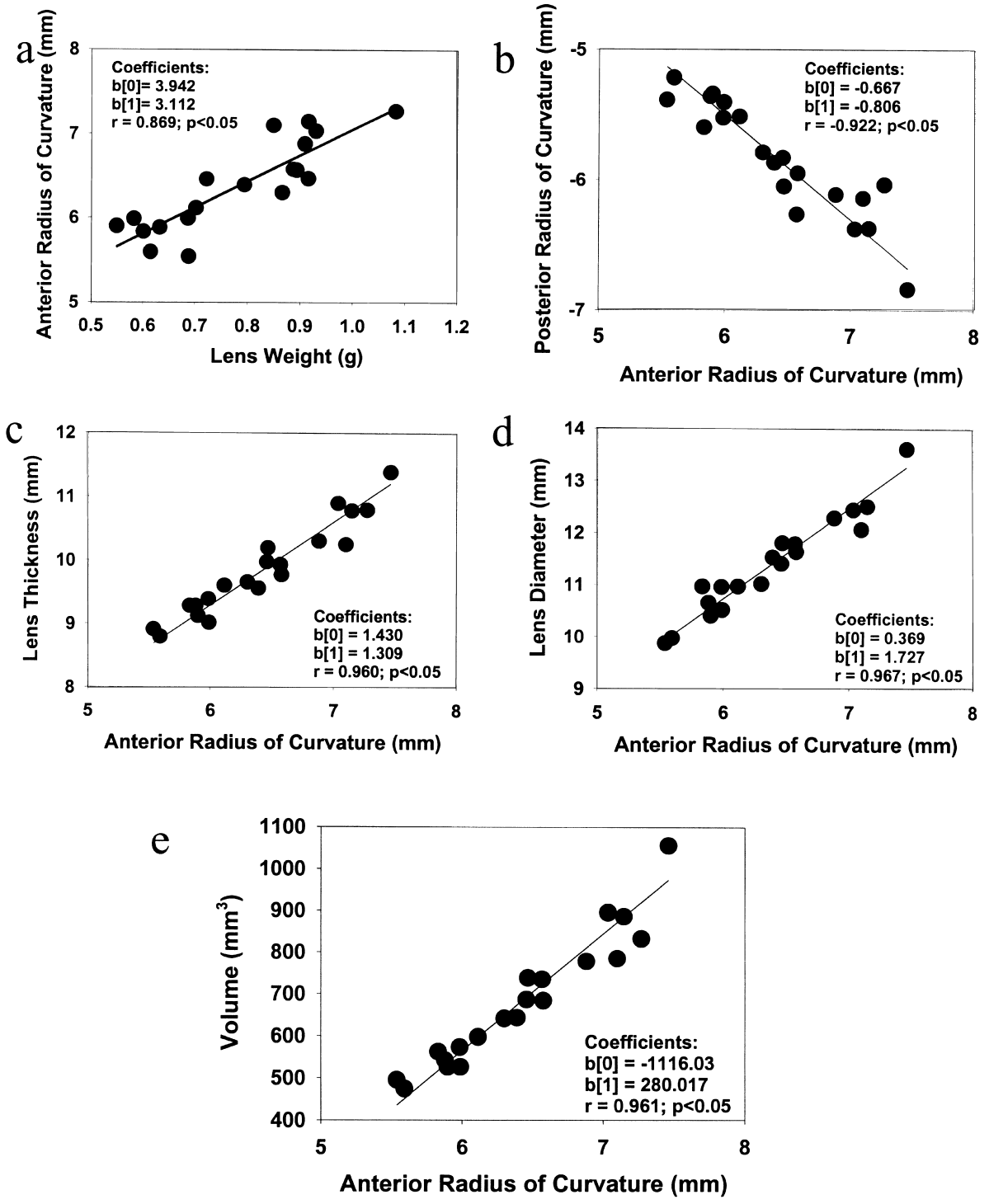

Figure 3. Linear relationships between various biometric properties of pig lenses as determined from orthogonal regressions. Lens weight (a), thickness (c), diameter (d) and volume (e) are all linearly related to lens anterior radius of curvature. Lens anterior and posterior radii of curvature are linearly related (b). All these parameters are also linearly related to posterior radius of curvature (not shown). In addition, since the anterior radius is linearly related with these parameters, correlations exist among thickness, diameter, posterior radius, weight and volume as well (not shown).

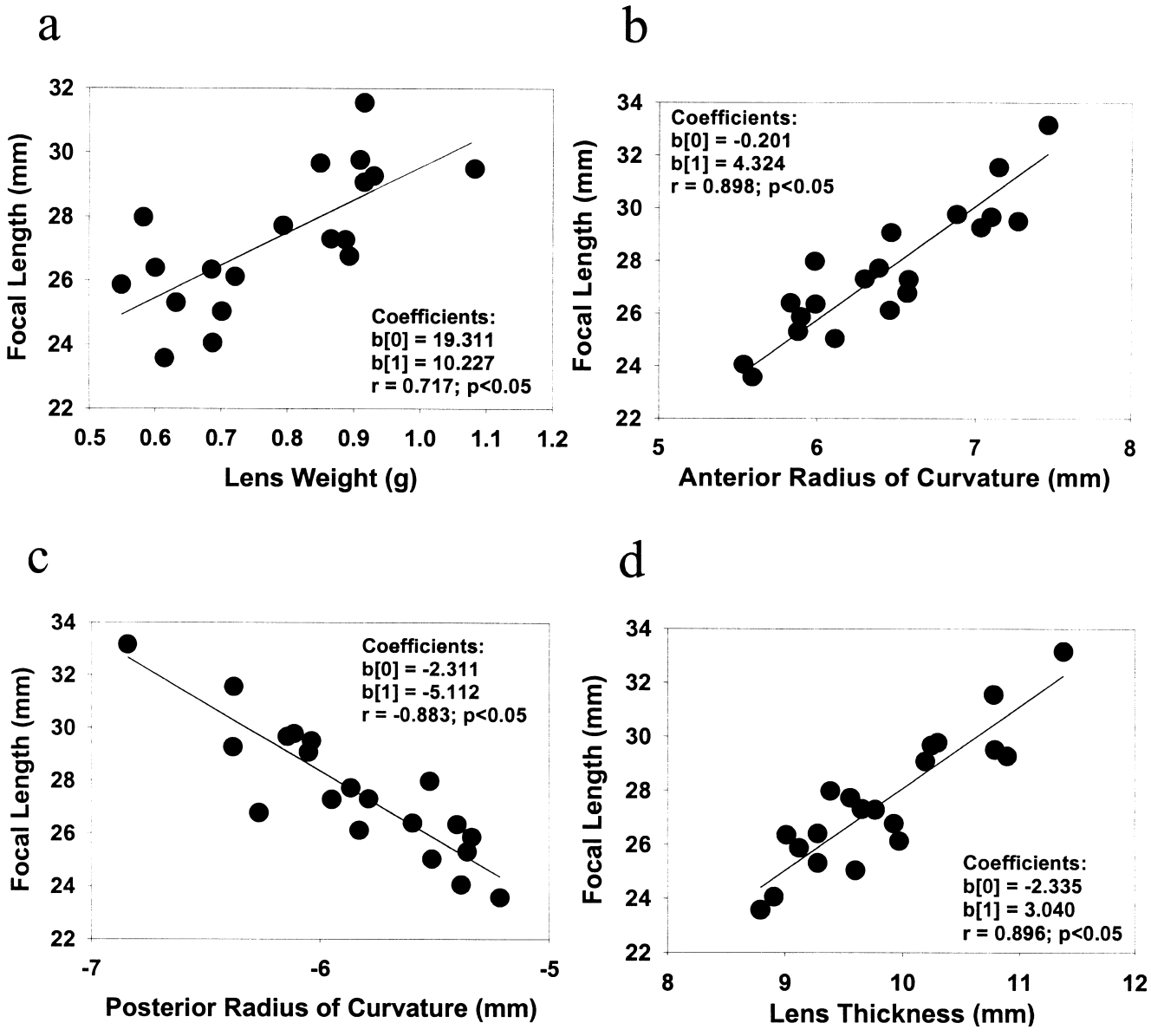

Figure 4. Significant linear relationships between lens focal length and weight (a), anterior radius of curvature (b), posterior radius of curvature (c) and lens thickness (d) as determined from orthogonal regressions. The graphs indicate that with increasing weight (and therefore age) the focal length increases due to increasing anterior and posterior radii of curvature and increasing thickness of the pig lens.

lens diameter increases, there is a significant linear increase in both the anterior radius of curvature (*Figure 3d*) and from Eq. (7), therefore also a significant linear increase (of negative sign) in posterior radius of curvature.

Relationships between the optical and biometric properties

In addition to the increase in lens focal length with increasing weight (*Figure 4a*), there are significant linear increases in focal length with an increase in anterior radius of curvature (*Figure 4b*), posterior radius of curvature (*Figure 4c*), lens equatorial diameter (*Table 1*) and lens thickness (*Figure 4d*).

Lens paraxial properties

While the measured total focal lengths of the lenses show highly significant orthogonal correlations with the lens biometric properties, the lens paraxial focal lengths show only marginally significant correlations with the same biometric properties (*Table 1*). The orthogonal correlation between total focal length and paraxial focal

length with a slope of 0.692 and an intercept of 10.480 shows that paraxial and total focal lengths are approximately equal at roughly 33 mm, but for focal lengths less than 33 mm, the total focal length is increasingly longer than the paraxial focal length. This might suggest that the negative spherical aberration increases systematically with decreasing focal length, but no significant relationship holds between spherical aberration and focal length (see below).

Equivalent and paraxial refractive indices of the lens

The mean equivalent refractive index for all the lenses measured was 1.4955 ± 0.0066 and the mean paraxial refractive index was 1.5197 ± 0.0266. The paraxial refractive index as calculated from the paraxial focal length shows a significant orthogonal correlation with the paraxial focal lengths such that with increasing paraxial focal length there is a decrease in the paraxial refractive index of the lens (*Table 1*). The total focal length and total refractive index do not show a significant correlation. No other significant correlations between either equivalent or paraxial refractive index with other biometric and optical properties of the lens were found.

The calculated mean equivalent refractive index value obtained from all lenses (1.4955) was used to calculate focal length of each individual lens using the thick lens equation (Eqs. (2), (3) and (4)). Kreuzer and Sivak (1985) previously calculated the equivalent refractive index of the pig lens to be 1.5088. This value was also used to calculate the focal length of the pig lenses used here. The paraxial refractive index of 1.5197 which was obtained in this study was also used to calculate the focal length. The focal lengths calculated from the three refractive indices were individually tested against the measured total focal length using a difference versus mean analysis, wherein the difference between the calculated focal length and measured focal length was tested against zero. If the calculated focal length predicts the measured focal length, then the mean of the differences should not be significantly different from zero. The focal length calculated from our total refractive index is not different from the measured focal length ($t = 0.361$ and $p = 0.722$) but the focal lengths calculated using the refractive index calculated by Kreuzer and Sivak (1985), and those calculated using our paraxial refractive index are different from the measured focal lengths ($t = -8.587$ and $p < 0.001$; $t = -14.089$ and $p < 0.001$ respectively). The equivalent refractive index value of the pig lens estimated by Kreuzer and Sivak (1985) is significantly different from our equivalent refractive index value ($t = 8.986$: $p < 0.001$) but is not significantly different from our paraxial refractive index value ($t = 1.830$: $p = 0.083$). A comparison of weight vs equivalent refractive index for the 20 lenses shows no significant relationship.

Spherical aberration of the lenses

Considerable variability in the spherical aberration of individual pig lenses was seen. Second and higher order polynomial curves were used to fit the complex relationships between focal length and lens diameters. To determine which power terms should be included in the model for each lens, we started with a large set of powers, from first to the tenth power, and then choose the best subset of the predictors having high R-square and low C–p indicators (SAS statistical software). The actual regression on these chosen power terms showed the significance level for each term. Those, if any, that did not contribute significantly to the regression were deleted and the regression was again done on the revised subset of terms. Finally, the normality of residuals (centered at zero) from regression confirmed the goodness-of-fit. Although the data from some lenses were significantly fit with polynomials of low order terms, reflecting only low order aberrations (2nd or 4th order terms), other spherical aberration curves could only be significantly fit with polynomials including higher (6th–10th) order terms (*Figure 5a–c*). Sixteen out of 20 of the pig lenses were found to have negative spherical aberration. No significant correlations between spherical aberration and any of the other measured or calculated variables were found. The mean spherical aberration for all pig lenses was -7.36 D $\pm$ 10.05 SD.

Geometrical relationships, lens volume and density

The calculated lens volume showed significant correlation with weight of the lens (*Table 1*). Since weight was well correlated with the other optical and biometric properties it follows that volume too shows similar significant correlations with these properties as shown in *Table 1* (*Figure 3e*). The mean calculated density of the pig lens was 1.183 kg/l (min = 1.018 kg/l, max = 1.390 kg/l). The density of the lenses as determined from the ratio of measured weight and calculated volume showed no significant correlation with equivalent refractive index or with paraxial refractive index.

Lens modeling

Since the lens biometric parameters (weight, curvature, thickness and diameter) are all significantly correlated with each other, this suggested that these parameters all constitute a purely geometrical relationship. This was tested using one of two lens models employing the equivalent refractive index and either the anterior radius of curvature (anterior radius model) or the thickness (thickness model) (*Figure 2*). The other parameters that were required to fully define the lens optical properties (*anterior radius model*: posterior radius, thickness; *thick-*

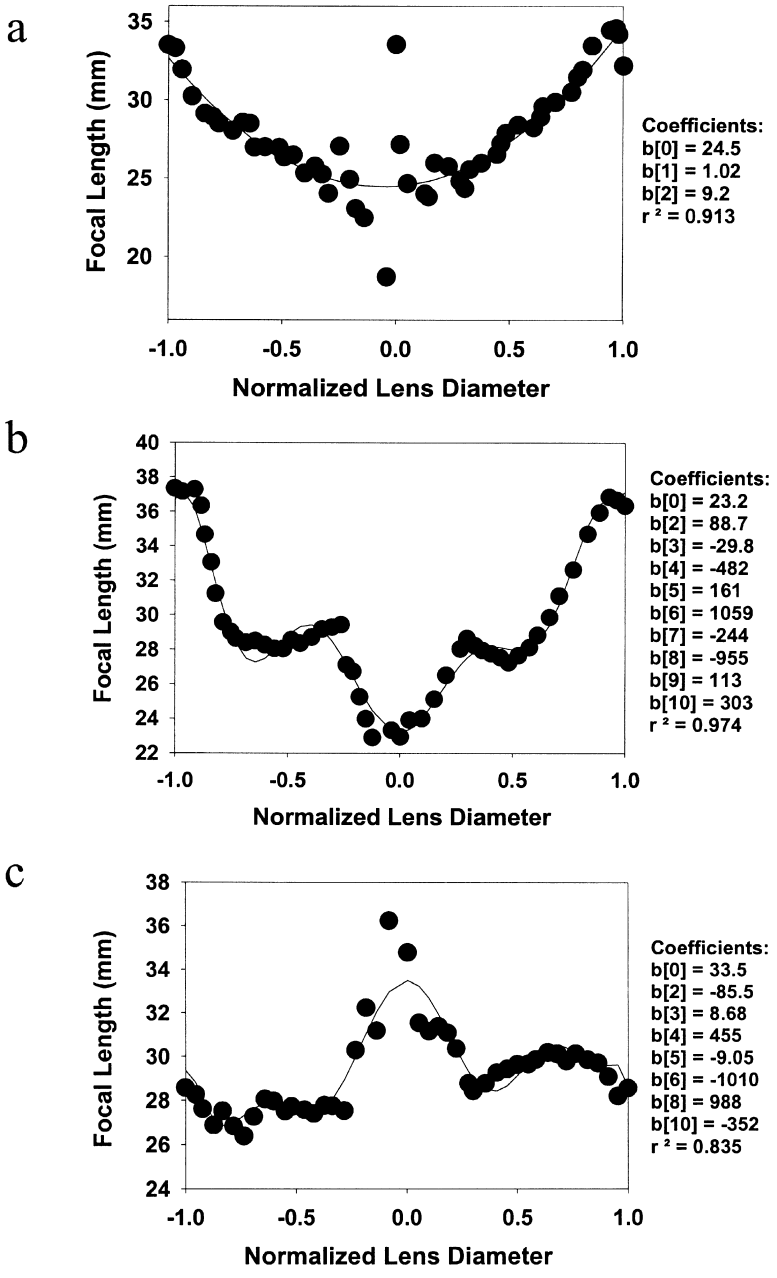

Figure 5. Spherical aberration graphs for three different pig lenses. The data are significantly fit with 2nd order (a) or higher order polynomial including up to 10th order terms ((b) and (c)). A wide variety of different patterns and extents of spherical aberration were seen in the pig lenses ranging from negative ((a) and (b)) to positive spherical aberration (c).

ness model: anterior radius and posterior radius) were obtained from the orthogonal regression equations relating anterior radius (for anterior model) or thickness (for thickness model) to these other parameters. The output values from both the anterior radius model and the thickness model were the geometrically calculated lens diameters and the focal lengths calculated from Eqs. (2), (3) and (4).

These diameters and focal lengths calculated from the two models were compared with the measured diameters and focal lengths. When the measured and modeled values were plotted together, a slope of one and intercept of zero indicates that the two measured and modeled parameters are not significantly different. The anterior radius model accurately predicts the measured lens diameters (slope tested against one, $t = -1.03$, $p = 0.317$; intercept tested

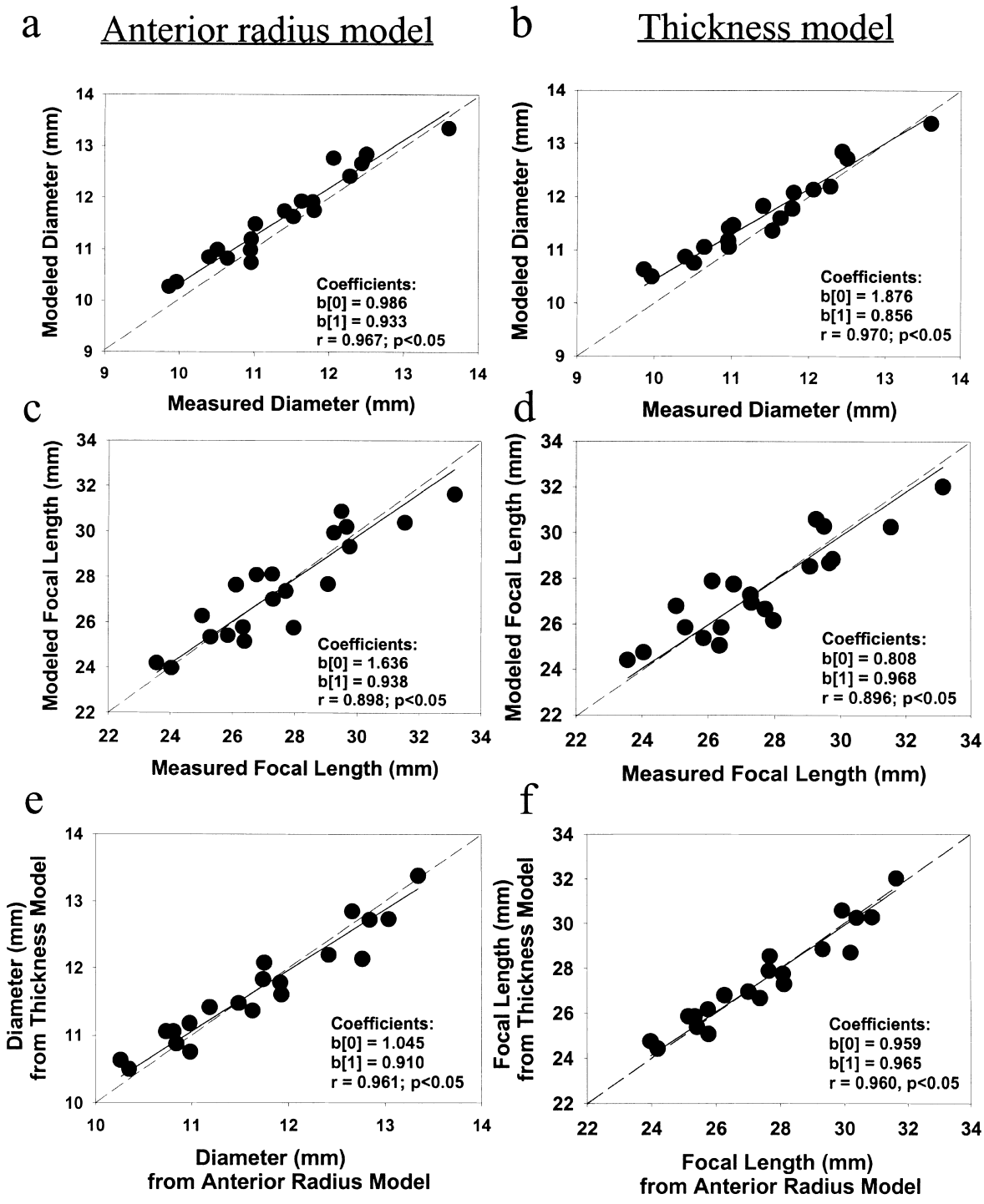

Figure 6. Relationships between measured and modeled diameters and focal lengths from the anterior radius lens model ((a) & (c)) and for the thickness lens model ((b) and (d)) for all pig lenses used. The modeled values are plotted on the y-axis and the measured values on the *x*-axis. The data are fit with orthogonal regressions. Comparisons between the measured and modeled diameters from the two models show significant linear relationships, but in the thickness model the slope and intercept differ significantly from the one-to-one line (dashed lines), but not in the anterior radius model ((a) and (b)). Comparisons between measured and modeled focal lengths from the two models show that the modeled focal lengths are not statistically different from measured focal lengths ((c) and (d)). Diameters and focal lengths obtained from thickness model and the anterior radius model are shown to produce essentially identical results ((e) and (f)).

against zero, $t = 1.33$, $p = 0.20$) (*Figure 6a*). However, the thickness model does not accurately predict the measured lens diameters (slope tested against one, $t = -2.42$, $p < 0.05$; intercept tested against zero, $t = 2.77$, $p < 0.05$) (*Figure 6b*).

The lens focal lengths calculated from the anterior radius model and the thickness model using the thick lens equation and assuming the mean equivalent refractive index value were plotted against the measured focal lengths (*Figures 6c,d*). These graphs show accurate predictions of the measured lens focal lengths both for the anterior radius model (slope tested against one, $t = -0.496$, $p = 0.626$; intercept tested against zero, $t = 0.474$, $p = 0.641$) and for the thickness model (slope tested against one, $t = -0.214$, $p = 0.833$; intercept tested against zero, $t = 0.195$, $p = 0.848$).

Lens diameters and focal lengths from the two models were plotted against each other. The diameters (slope tested against one, $t = -1.245$, $p = 0.229$; intercept tested against zero, $t = 1.236$, $p = 0.232$) and focal lengths (slope tested against one, $t = -0.453$, $p = 0.656$; intercept tested against zero, $t = 0.454$, $p = 0.655$) (*Figures 6e,f*) as obtained from the two models show that they are not statistically different from each other.

Discussion

Correction of the measured data

As mentioned, the data presented have been corrected based on measurements of precision ball bearings. Had this systematic error been detected prior to undertaking the study, an appropriate correction would have been applied to the image calibration, but the end result would have been identical. The error was detected when the calculated lens densities were found to be too high. After correction, the calculated lens densities, although in a few cases still high, are as a whole far more realistic. In retrospect, the lens densities should have been determined from direct measurements of lens volume through a simple fluid displacement method. However, this was not done. One additional lens in which surface curvatures were measured using the corrected image calibrations and for which density was calculated from a direct measurement of volume through fluid displacement, showed a good agreement between density calculated from the digitized surface measurements and density calculated from the direct volume measurement. We therefore feel that the corrected measurements accurately reflect the actual lens dimensions.

Interrelationships between biometric properties of the lenses

The surface curvatures of the porcine lens are spherical in contrast to the human lens surface curvatures. Since the points that are marked on the anterior and posterior lens surfaces all the way to the lens equator are well fit by spherical curves, we feel that we are justified in describing both the anterior and posterior lens surface curvatures as spherical. This is an unusual finding for the surface curvatures of a mammalian crystalline lens, but since no such comprehensive studies have previously been done on the pig lens, no comparisons can be made with previous data. All the biometric and optical properties of the pig lenses show significant correlations with weight and with calculated lens volumes within the range of weights and hence within the age range of pig lenses obtained. In isolated human lenses, while the weight increases linearly with age, the anterior radius of curvature, posterior radius of curvature and focal length show a change at about age 65 (Glasser and Campbell, 1999). However, in spite of the nonlinearity of these relationship as a function of age in human lenses, the linear relationships between anterior radius of curvature and focal length, between posterior radius of curvature and focal length, and between anterior and posterior radii of curvature are still present in the human lens (Glasser and Campbell, 1999), just as they are found here for the porcine lens. This is especially noteworthy since a fundamental difference between the porcine lens and the human lens is that the human lens accommodates in youth while the pig almost certainly does not (Hughes, 1977; Duke-Elder, 1958; Walls, 1967). Thus, the isolated, young human lens must be considered as being in an accommodated form upon removal from the eye due to the absence of zonular tension (Glasser and Campbell, 1998, 1999). The three linear relationships mentioned above that were found in human lenses considers young-accommodated and older-unaccommodated human lenses. In the case of the pig, the relationships are all for lenses in the same unaccommodated state (since the pig is unlikely to accommodate). The similar relationships found for pig and human lenses suggest the existence of generalized optical and physical developmental constraints on the crystalline lenses of at least these two mammalian species. This hypothesis is given further support from the existence of significant linear relationships between the otherwise apparently unrelated lens focal lengths and diameters of both human and pig lenses. Glasser and Campbell (1999) remarked on this unusual relationship for the human lens which lack the obvious geometric structure (i.e. spherical surfaces) of the pig lens. However, the underlying theme suggested by this relationship between focal length and lens diameter in both pig and human lenses is that the biometric properties of the lens may dictate the optical characteristics. The existence of the surprisingly strong linear relationship between focal length and lens diameters in both the human and pig lens suggest that the optical and biometric properties are codependent. Mutti *et al.* (1998) discuss a possible developmental model for the human lens in childhood in which increasing equatorial expansion of the globe serves to regulate lens power to

maintain emmetropia by stretching and thinning the lens. The linear relationship between focal length and diameter for human lenses of all ages and for pig lenses suggest the possibility that this model may be age independent and more universally applicable.

The measured thickness and equatorial diameters of the pig lenses also show significant correlations with other properties. Pig lenses therefore becomes thicker, larger in diameter, flatter in surface curvatures and reduced in power as age advances within the range covered by this study. The significant correlations between various optical and biometric parameters of the pig lens (most r values lying between 0.452 and 0.989) and the relatively good predictability of the lens models suggest that the physical properties of the pig lens may adhere to a pre-determined developmental course.

Density of the pig lens

The calculated mean density of the porcine crystalline lens (1.183 kg/l) is statistically different from a value of 1.113 reported by Scammon and Hesdorffer (1937) for the human crystalline lens ($t = 2.52$, $p = 0.021$). The specific gravity of the human crystalline lens as measured by Smith (1883) varies between 1.067 (20–29 years) to 1.090 (80–90 years), while Scammon and Hesdorffer (1937) show specific gravities ranging from 1.034 (20 year olds) to 1.113 (90 year olds). Some of the pig lenses in our study had higher than expected densities, possible due to overestimation of the true lens weight as a consequence of having measured lens wet weight. This measurement may have included excess moisture and possibly some vitreous and remnants of ciliary body tissue still adhering to the lens. However, it is also possible that the true density of the pig lens may be greater than that of the human lens. This may not seem unreasonable since: (a) as assessed subjectively, the pig lens is harder than a young primate lens, (b) the pig lens has no requirement to accommodate and hence may be more dense than an accommodating lens and (c) the equivalent refractive index of the pig lens, as determined here at least, is considerably greater than that of the human lens and may be expected to increase with increased density (although calculated density and equivalent refractive index of the pig lenses was not significantly correlated).

Nunneley (1858) measured densities of lenses from different species and found the mean density of the pig lens to be 1.0969 (1.0864–1.1060) and the human lens was found to be 1.1121 (1.0909–1.1304). Nunneley's mean density and density range for the pig lens are not different from his range of densities in human lens. Dry weight has also been used as an indicator of the original water content of the lens and as an indicator of the lens density. Klethi and Mandel (1965) measured dry weight for the pig lens to be 60% and others have measured the dry weight to be 73.8% (Kuck, 1975). The dry weight of human lens was measured to be 69.2% ± 0.7 (Maraini and Mangili, 1973) which is within the range of the water content reported for the pig lens.

Together, this data suggests that despite the fact that the pig most likely does not have an accommodating lens and has a lens that may be harder than the young human lens, the densities of pig and human lenses are unlikely to be different and our calculations reported here may have slightly overestimated the pig lens densities. Clearly, direct measurements are a more appropriate method for obtaining lens densities and calculations as performed here may be more prone to error.

Refractive index

According to our measurements, the mean equivalent refractive index of the pig lens was 1.4955 and the mean paraxial refractive index was 1.5197. The value of 1.5088 from Kreuzer and Sivak (1985) is significantly different from our equivalent value, but is not significantly different from our paraxial refractive index value. Equivalent and paraxial refractive indices show no change with weight in the lenses measured although the lens focal length and radii of curvature do. Therefore, the equivalent and paraxial refractive indices show no systematic age related change. It is interesting to note that the calculated density of the pig lens has no relationship with either equivalent or paraxial refractive index of the lens, but changes in density are certainly likely to affect the refractive index gradient.

Spherical aberration

The extent of spherical aberration was obtained by fitting a polynomials to the points of intersection of the exit beams with the optical axis of the lens. In the case of human lenses, forth order polynomials provided adequate fits for all lenses (Glasser and Campbell, 1998). This was not the case for the pig lenses. In pig lenses the polynomials included terms ranging from 2nd to 10th order to encompass the large variability in aberrations between different lenses (*Figure 5*). Spherical aberration in the human lens showed a significant linear correlation with age (Glasser and Campbell, 1998) but spherical aberration of the porcine lens was not correlated with any of the parameters measured. The sign of the spherical aberration, predominantly negative for the pig lenses, also did not show any relationships with any of the other parameters.

Optical aberrations of the pig lens

In the human lens the paraxial focal length shows significant correlations with other optical and biometric parameters (Glasser and Campbell, 1998, 1999). However, in the pig lens, while the paraxial focal length does show significant correlations with some optical and

biometric parameters, the total focal length shows stronger relationships with the same parameters. Since the porcine lens surface curvatures are spherical, unlike that of human lenses, the total focal length therefore seems to serve as a better measure of optical property of the lens than the paraxial focal length. The nonsystematic sign and extent of the spherical aberrations of different pig lenses contributes to the nonsystematic variability between the paraxial focal length and the total focal length.

That the discrepancy between the paraxial and the total focal lengths of the pig lenses is real is evident from the aberrations of the pig lenses. Based on the spherical aberration plots, some lenses do not have conventional spherical aberration, but have higher order aberrations. The significance of this finding is difficult to interpret. It is as likely due to real aberrations as it may, for example, be due to the lenses having been subjected to temperature extremes during shipping. It is unlikely to result from handling and dissections in the laboratory since the aberrations are generally symmetric about the optical axis. Whether or not these lenticular aberrations have any functional significance for pig vision, is unclear. A large proportion of the lens surface that is available to laser scanning optical analysis is not available to vision since it is obscured by the pupil *in vivo*.

It is tempting to suggest that the pig lens may have multifocality to compensate for the chromatic aberration as has been shown in other species (Kröeger *et al.*, 1999). The mean spherical aberrations in twenty lenses measured was $-7.36\,\mathrm{D} \pm 10.05$ SD where as Kreuzer and Sivak (1985) showed only 3.57 D of chromatic aberration in the pig lens. This discrepancy suggests that the spherical aberration is not compensating for the chromatic aberration. Spherical aberration varies from positive to negative non-systematically and the data are significantly fit with curves containing 2nd–10th order coefficients, thus representing a high degree of inter-individual lens variability. Such non-systematic changes in the spherical aberration of different pig lenses suggest that it is unlikely that there is a systematic compensation of the chromatic aberration in the pig eye. While such multifocality, if this is what it is, may be beneficial in the absence of function accommodation, again, the considerable inter-individual variability in the sign and extent of the aberrations make it hard to conclude that this is a functional or evolutionary development in the pig lens to compensate for a lack of accommodation.

Without information on the whole eye aberrations, the possible compensatory aberrations from the cornea or anatomical information from the individual lenses, no unequivocal explanation as to the existence of a possible functional multifocality can be provided from this study. Perhaps future investigations of the gradient refractive index of the pig lens may lead to a better understanding of the possible etiology of these aberrations. Certainly, direct photorefractive examination of live pigs may identify if such multificality occurs naturally.

Modeling the lens

Owing to the significant correlations between biometric and optical properties and the sphericity of the lens surfaces, two geometric models of the porcine lens were derived from lens anterior radius of curvature and lens thickness. *In vivo*, the lens anterior radius of curvature and thickness lend themselves readily to accurate measurements from phakometry and a-scan ultrasonography respectively. Based on the models described here, this would allow an *in vivo* prediction of the lens focal lengths and diameters, from the surface curvature or thickness measurements alone. Therefore the regression equations relating anterior radius to posterior radius, thickness, diameter and focal length (anterior radius model) and regression equations relating lens thickness to anterior radius, posterior radius, diameter and focal length (lens thickness model) were used. The anterior radius model provide reasonable predictions of the lens focal lengths and diameters, but the thickness model is relatively poorer at predicting the diameter, thus rendering this approach less appropriate (*Figure 6*). The consistency of the models was determined qualitatively by comparing the diameters and focal lengths from both models. Although the focal lengths are predicted by the two models, this could possibly have occurred through duplication of errors. While the thickness model does not predict diameter well, the diameters from the two models agree, possibly because both model diameters deviate slightly from the true diameters such that when compared against each other the two agree.

An accurate model of the porcine lens would predict the optical and surface characteristics of the lens in vivo provided that the surface characteristics do not change when the lens is removed from the eye. In the case of the pig lens, a systematic change in the lens shape is unlikely to occur since the pig lens almost certainly has no accommodation (Hughes, 1977; Duke-Elder 1958; Walls, 1967). Ideally, the predictive ability of this model would have been tested by measuring lens thickness or anterior surface curvature in intact pig eyes and then removing the lens from the eye and verifying the predictions. This has yet to be done to further validate the model, but is beyond the scope of the current study.

A similar relationship between surface curvatures and focal length found here for the pig lenses was also found in isolated human lenses (Glasser and Campbell, 1999). The question may arise as to whether a similar modeling approach could be used for predicting the human lens power from *in vivo* surface curvature or thickness measurements from phakometry or a-scan ultrasonography respectively. Certainly, extrapolation from this study on a limited

number of lenses from a different species provides no sound justification for this in humans. In addition, the possibility of predicting human lens power from surface curvature measurements *in vivo*, may be complicated by the fact the young human lens must be considered to be accommodated when removed from the eye and further, the apparent existence of a 'lens paradox' in the human eye (Brown, 1974; Koretz and Handelman, 1986, 1988) may complicate this. However, the linear relationship between surface curvatures and focal length for human lenses (Glasser and Campbell, 1999), as found here for pig lenses, suggests no paradox between focal length and surface curvatures, at least for these limited data sets.

Since no information is available on the age of the pig lenses used in this study, the increasing weights are considered to reflect the growth of the lenses. Since the biometric properties are linearly related for this group of pig lenses of different weights, growth changes in one parameter do not occur independent of the other parameters. The growth of the pig lens must therefore follow a pattern with the result that older lenses are essentially scaled up versions of the younger lenses. Modeling the lens has allowed an examination of the geometric nature of the relationship between the various optical and biometric properties and has provided some understanding of the growth and developmental constraints of the lens. The relative similarity between the results obtained from the anterior radius model and the thickness model demonstrate the consistency of these models. The implications of this are that the geometry, biometric and optical characteristics of pig lenses *in vivo* can with reasonable accuracy be predicted from the anterior radius of curvature or the thickness of the lens alone. Certainly, a better prediction of the lens geometry and focal length is available from the lens anterior radius of curvature. If the pig lens optical properties *in vivo* are to be predicted, this study suggests this can best be accomplished from *in vivo* measurements of the lens anterior radius of curvature.

Future design of intraocular lenses to be tested in pig eyes, such as those created by injecting polymers through a small diameter capsulorhexis (Hettlich *et al*., 1994) may be made to conform to the original lens optical and biometric properties by taking account of the data presented here. We have, for this reason, included values for slopes and intercepts for all linear relationships identified to allow such possible future use of this data. The linear relationship between the volume of the lens and the anterior radius of curvature or lens thickness, for example will prevent overfilling or underfilling of the lens capsular bag since volume can be predicted. Should similar relationships be found for other primate lenses, this may be useful for prevention of under-filling of polymer intraocular lenses as has been reported previously in monkey eyes (Nishi *et al.*, 1997).

Gradient refractive index optics

The spherical surface curvatures, the well defined geometrical and optical relationships and the geometrical scaling of the pig lens with increasing weight (and therefore age) make it good candidate for further studies of the gradient refractive index of the lens. Prior modeling of the crystalline lens relating impirical and experimental measurements of lens aberrations has been limited to spherical lenses which allow concentric isoindical models of the gradient refractive index to be calculated (Campbell, 1984; Axelrod *et al.*, 1988; Kröeger *et al*., 1994). While the pig lens is not spherical in shape, the spherical surface curvatures would allow isoindical layers of the lens to be constructed for the anterior and posterior caps. Although refractive index discontinuities between the anterior and posterior caps at the lens equator must still be addressed, a number of complexities are eliminated when using lenses that conform to the geometrical relationships shown here. Together with the predictive ability of such models and comparison of the computed and measured spherical aberration, the data presented here may allow for more empirically based gradient refractive index models of the mammalian lens to be calculated than have previously been available for non-spherical lenses.

Conclusion

Interrelationships between various parameters of the pig lens have been measured and quantified and relationships between these parameters have been established. The significant linear relationships between many of these parameters suggest the growing pig lens conforms to a generalized geometrical structure and the optical and physical development of the lens are codependent. The results presented here facilitate the construction of a geometric model of the pig crystalline lens and the validity of this generalized model is confirmed by the agreement between calculated and measured focal lengths. Knowledge of these geometrical relationships may be useful for future studies which use pig lenses to explore the possibilities for design of polymer intraocular lenses. These empirical measurements of the pig lens may facilitate future studies of the gradient refractive index of the mammalian lens and allow comparisons between the measured and modeled optical properties.

Acknowledgements

We thank Dr Austin Roorda for use of laboratory space, Dr Hu for statistics consultation and the helpful comments from the two anonymous reviewers. This work was funded in part by a grant from Pharmacia, Groningen BV to AG.

References

Axelrod, D., Lerner, D. and Sands, P. J. (1988). Refractive index within the lens of a goldfish eye determined from the paths of thin laser beams. *Vis. Res.* **1,** 57–65.

Brown, N. P. (1974). The change in the lens curvature with age. *Exp. Eye. Res.* **19,** 175–183.

Campbell, M. C. W. (1984). Measurement of refractive index in an intact crystalline lens. *Vis. Res.* **24,** 409–415.

Coile, D. C. and O'Keefe, L. P. (1988). Schematic eyes for domestic animals. *Ophthal. Physiol. Opt.* **8,** 215–220.

Duke-Elder, S. (1958). The eye in evolution. In: *System of Ophthalmology*, Vol. 1, Henry Kimpton, London, UK, p. 653.

Glasser, A. and Campbell, M. C. W. (1998). Presbyopia and the optical changes in the human crystalline lens with age. *Vis. Res.* **38,** 209–229.

Glasser, A. and Campbell, M. C. W. (1999). Biometric, optical and physical changes in the isolated human crystalline lens with age in relation to presbyopia. *Vis. Res*. **39,** 1991–2015.

Hara, T., Hara, T., Yasuda, A. and Yamada, Y. (1990). Accommodative intraocular lens with spring action. Part 1: Design and placement in an excised animal eye. *Ophthal. Surgery* **21,** 128–133.

Hettlich, H. J., Lucke, K., Asiyo-Vogel, M. N., Schulte, M. and Vogel, A. (1994). Lens refilling and endocapsular polymerization of an injectable intraocular lens: *In vitro* and *in vivo* study of the potential risks and benefits. *J. Cataract Ref. Surg.* **20,** 115–123.

Hughes, A. (1977). The visual system in vertebrates. (ed F. Crescitelli), In: *Handbook of Sensory Physiology*, Vol. 7(5), Springer-Verlag, New York, p. 676.

JMP Statistics and Graphics Guide, *Version 4* (2000), SAS Institute Inc., Cary, NC, USA

Klethi, J. and Mandel, P. (1965). Eye lens nucleotides of different species of vertebrates. *Nature* **205,** 1114–1115.

Koretz, J. F. and Handelman, G. H. (1986). The lens paradox and image formation in accommodating human eyes. *Topics Aging Res. Europe* **6,** 57–64.

Koretz, J. F. and Handelman, G. H. (1988). How the human eye focuses. *Sci. American* **259,** 92–99.

Kreuzer, R. O. and Sivak, J. G. (1985). Chromatic aberration of the vertebrate lens. *Ophthal. Physiol. Opt.* **5,** 33–41.

Kröeger, R. H. H., Campbell, M. C. W., Fernald, R. D. and Wagner, H. J. (1999). Multifocal lenses compensate for chromatic defocus in vertebrate eyes. *J. Comp. Physiol. A* **184,** 361–369.

Kröeger, R. H. H., Campbell, M. C. W., Munger, R. and Fernald, R. D. (1994). Refractive index distribution and spherical aberration in the crystalline lens of the African cichlid fish *Haplochromis burtoni*. *Vis. Res.* **34,** 1815–1822.

Kuck Jr, J. F. R. (1975). Composition of the lens. In: *Cataract and Abnormalities of the Lens* (ed J. G. Bellows), Grune & Stratton, Inc, New York, p. 69.

Kuszak, J. R. and Brown, H. G. (1994). Embryology and anatomy of the crystalline lens. In: *The Principles and Practice of Ophthalmology: Basic Sciences* (eds D. M. Albert and F. A. Jacobiec), W.B. Saunders, Philadelphia, pp. 82–96.

Maraini, G. and Mangili, R. (1973). Differences in proteins and in the water balance of the lens in nuclear and cortical types of senile cataract. In: *The Human Lens—In Relation to Cataract, Ciba Foundation Symposium 19* (eds K. Elliott and D. W. Fitzsimons), Associated Scientific Publishers, Amsterdam, p. 82.

Masajada, A. P. (1999). Numerical study of the influence of the shell structure of the crystalline lens on the refractive properties of the human eye. *Ophthal. Physiol. Opt.* **1,** 41–49.

Mutti, D. O., Zadnik, K., Fusaro, R. E., Friedman, N. E., Sholtz, R. I. and Adams, A. J. (1998). Optical and structural development of the crystalline lens in childhood. *Invest. Ophthal.* **39,** 120–133.

Nakao, S., Fujimoto, S., Nagata, R. and Iwata, K. (1968). Model of refractive-index distribution in the rabbit crystalline lens. *J. Opt. Soc Am. A.* **58,** 1125–1130.

Nakao, S., Ono, T., Nagata, R. and Iwata, K. (1969). The distribution of refractive indices in the human crystalline lens. *Jap. J. Clin. Ophthalmol.* **23,** 903–906.

Nishi, O., Nishi, K., Mano, C., Ichihara, M. and Honda, T. (1997). Controlling the capsular shape in lens refilling. *Arch Ophthalmol.* **115,** 507–510.

Nunneley, T. (1858). On the form, density and structure of the crystalline lens. *Quart. J. Micr. Sci.* **6,** 136.

Pierscionek, B. K. and Augusteyn, R. C. (1992). Growth related changes to functional parameters in the bovine lens. *Biochimica et Biophysica Acta* **1116,** 283–290.

Scammon, R. E. and Hesdorffer, M. B. (1937). Growth in mass and volume of the human lens in postnatal life. *Arch.Ophthal.* **17,** 104–112.

Sivak, J. G. and Kreuzer, R. O. (1983). Spherical aberration of the crystalline lens. *Vis. Res.* **23,** 59–70.

Smith, P. (1883). Diseases of crystalline lens and capsule. *Trans. Ophthal. Soc. U.K.* **3,** 79–99.

Walls, G. L. (1967). *The Vertebrate Eye and its Adaptive Radiation*, Hafner Publishing Company, New York, p. 285.